JOURNAL OF AIRCRAFT
Vol. 45, No. 3, May–June 2008

Wind-Tunnel Testing of Rotor with Individually Controlled Trailing-Edge Flaps for Vibration Reduction

Beatrice Roget*
National Institute of Aerospace, Hampton, Virginia 23606
and
Inderjit Chopra†
University of Maryland, College Park, Maryland 20742

DOI: 10.2514/1.28455

A control method is proposed to reduce vibrations in helicopters using active trailing-edge flaps on the rotor blades. Each blade is controlled independently, taking into account possible blade dissimilarities. The method consists of performing simultaneous system identification and closed-loop control at each time step. For the system identification, different inputs are applied to each blade, and the relationship between the individual blade inputs and the resulting loads in the fixed frame is estimated on-line, assuming a linear-time-periodic model of the helicopter. Closed-loop tests are conducted using a four-bladed Mach-scaled rotor with piezobender trailing-edge flaps. The rotor model is fitted on a bearingless model-scale hub and tested in the Glenn L. Martin wind tunnel. These tests demonstrate the controller's ability to account for blade dissimilarities and generate different optimal inputs for each blade. The 1 and 4/rev components of fixed frame loads are reduced individually by 50 and 60%. Simultaneous reduction of 1 and 4/rev components is also demonstrated (43% reduction). However, vibration increases are noted for some nontarget hub loads.

Nomenclature

F	=	fixed frame hub vibration vector
H	=	measurement matrix
I	=	identity matrix
J	=	scalar nondimensional vibration objective function
K	=	Kalman gain vector
N_b	=	number of blades
N_h	=	number of harmonics
P	=	covariance of estimation error
Q	=	covariance of process noise
R	=	rotor radius (dimensional)
r	=	covariance of measurement noise
rev	=	rotor revolution
T	=	transfer matrix relating flap inputs to hub vibration
W_z	=	weighting matrix for fixed frame hub loads
W_γ	=	weighting matrix for control inputs
$W_{\Delta\gamma}$	=	weighting matrix for control input rates
x	=	state vector
z	=	measurement vector
γ	=	command input for trailing-edge flap
$\gamma_{\max}$	=	upper limit for command input
$\Delta\gamma$	=	flap actuation increment in 1 rev
δ	=	trailing-edge flap deflection
μ	=	advance ratio
Ω	=	rotor speed (dimensional)

Subscripts

k	=	blade number
n	=	iteration number
$()_0$	=	uncontrolled

Received 20 October 2006; revision received 19 November 2007; accepted for publication 20 November 2007.

*Research Scientist. Member AIAA.
†Alfred Gessow Rotorcraft Center Professor and Director, Department of Aerospace Engineering. Fellow AIAA.

I. Introduction

HIGH vibration levels limit helicopter performance and reduce the structural life of components. Most of the vibration in the helicopter originates from the main rotor. Oscillatory air loads are caused by a highly unsteady flowfield, complex wake structure, coupled and nonlinear blade motions, and time-varying blade pitch inputs. When the blades are identical (tracked rotor), only kN_b/rev harmonic loads occurring at the rotor hub are transmitted to the fuselage (where N_b is the number of blades and k is an integer). On the other hand, if the blades are not identical (dissimilar rotor), significant non-kN_b/rev loads are also transmitted to the helicopter fuselage.

Passive vibration reduction methods such as pendulum absorbers or modal placement methods have limited effectiveness over a narrow range of operating conditions. The most widely studied active control methods use multicyclic pitch excitation. These methods have great potential because they eliminate vibration at its source. They are implemented by actuating the rotor blades at higher harmonics to generate unsteady forces, which, when properly phased, counteract existing vibratory air loads. Several implementation techniques have been considered, such as HHC (higher harmonic control), IBC (individual blade control), and active control of trailing-edge flaps [1].

The HHC technique uses swash-plate actuation to control pitch angles of rotor blades. It has been demonstrated to reduce vibrations through numerical simulations [2], model, and full-scale wind-tunnel tests [3–5], as well as flight tests of full-scale vehicles [6]. However, the blades cannot be controlled individually. As a result, non-kN_b/rev harmonics arising from rotor dissimilarities cannot be controlled.

An extension of this technique uses blade root actuators in the rotating system to individually control each blade pitch (IBC). The potential of IBC to reduce vibration has been demonstrated for identical rotor blades both analytically [7,8] and experimentally [9,10]. Both HHC and IBC methods require a complex actuation system that impose a considerable weight penalty and induce high pitch link loads.

The introduction of smart material actuators has renewed interest for an alternative active vibration control approach that employs trailing-edge flaps [11–13]. These actuators are lightweight, compact, high bandwidth, and have a low power requirement. Active

Table 1 Mach-scaled model parameters

Parameters	Value
Rotor diameter	5 ft
Airfoil section	NACA0012
Airfoil chord	3 in.
Operating speed	1800 rpm
Tip speed	472 ft $\cdot$ s^{-1}
Flap span	2.4 in. (8% span)
Flap chord	0.6 in. (20% chord)
Radial location of flap	75% span

trailing-edge flaps have been shown to achieve a level of vibration reduction comparable with conventional IBC while using moderate input angles [14,15].

The IBC approach, either through complete blade feathering or using trailing-edge flap actuation, allows each blade to be controlled individually and can target the non-kN_b/rev loads. However, existing control methodologies do not make use of this capability. They use the same phase-shifted control inputs to all blades, assuming a tracked rotor (identical blades). Dissimilarities in helicopter blades can cause a tremendous increase in vibratory loads at the hub. Currently, to overcome this problem, blade tracking is performed periodically resulting in a significant increase in operating cost and helicopter down time. Moreover, to minimize blade dissimilarities, tight manufacturing tolerances are imposed leading to high manufacturing cost. Blade tracking and tight tolerances minimize vibrations, but they are time consuming and expensive.

Recently, closed-loop wind-tunnel tests on a 4-bladed Mach-scale rotor using piezobimorphs actuated trailing-edge flaps were conducted in the Glenn L. Martin wind tunnel [16]. This actuation system successfully minimized 4/rev hub loads by over 90% for steady and transient flight conditions. A neural network based adaptive controller was used where the controller assumed identical blades [17–19]. As a result, large 1/rev loads arising out of rotor dissimilarities could not be controlled. Any attempt to target these non-kN_b/rev loads led to excessive flap requirements. This resulted in the saturation of actuators and enormously degraded control performance. In the present study, a new control methodology is used which takes into account blade dissimilarities and reduces both kN_b and non-kN_b/rev loads [20]. In a previous paper, the method's potential to affect vibratory loads at multiple harmonics was demonstrated in hover [21]. This paper describes closed-loop vibration reduction tests conducted in forward flight in the Glenn L. Martin wind tunnel.

The paper is organized in three parts. In the first part, the control algorithm is described. In the second part, the active model rotor and experimental facilities used for the closed-loop tests are described. In the third part, results of closed-loop tests in forward flight are presented.

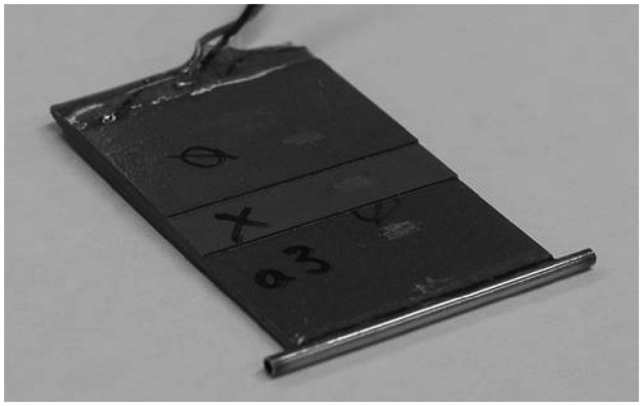

Fig. 1 Actuator.

II. Control Algorithm

A control algorithm is developed to achieve vibration reduction in the special case when the rotor blades have dissimilarities, resulting in non-kN_b/rev harmonics in the fixed frame hub vibratory loads. Different control inputs, respectively, generated for each blade can

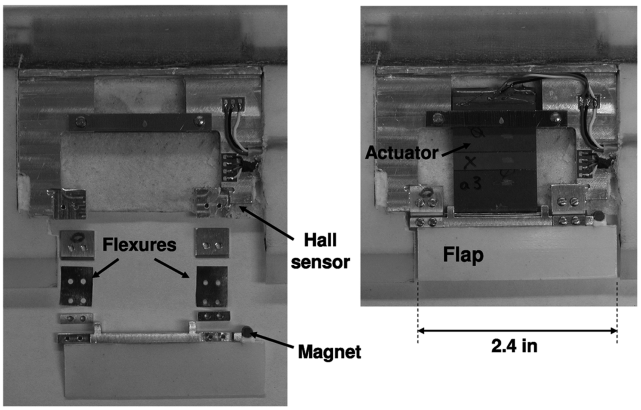

Fig. 2 Flap and actuator assembly.

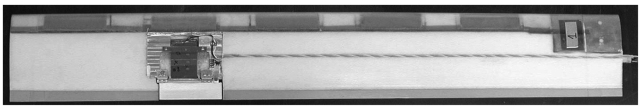

Fig. 3 Blade.

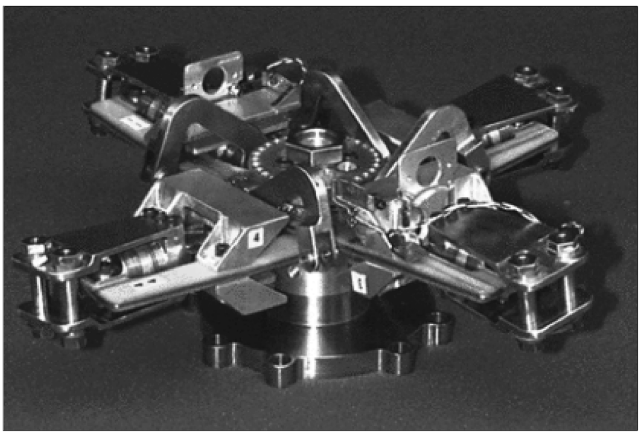

Fig. 4 Bell-412 Mach-scaled rotor hub.

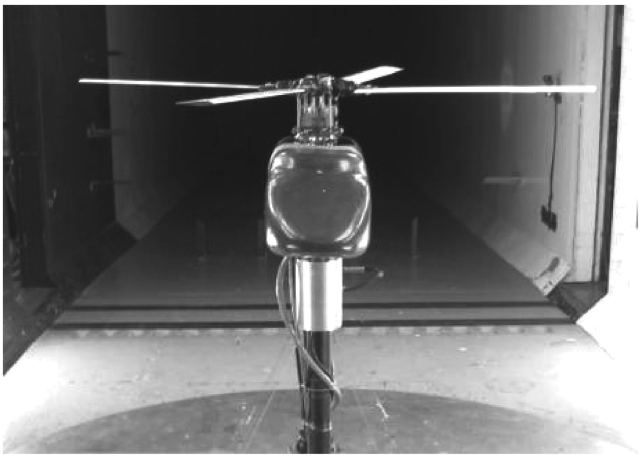

Fig. 5 Rotor installed in wind-tunnel section.

attempt to minimize both the baseline kN_b/rev vibration and the dissimilarity-induced non-kN_b/rev loads.

The linear quasi-static model relating the response vector F to the input vector γ through a transfer function is described as

$$F = F_0 + T\gamma \tag{1}$$

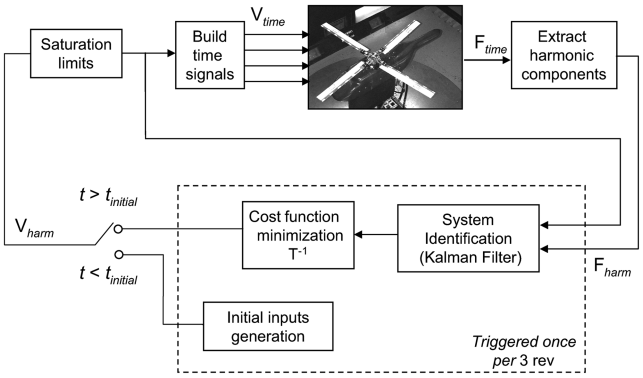

Fig. 6 Controller diagram.

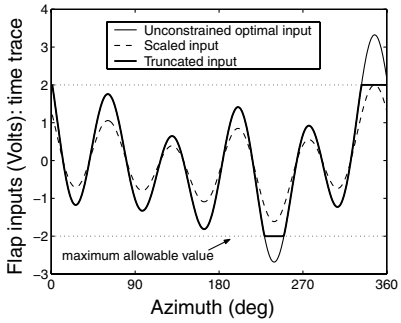

Fig. 7 Applying limits using scaled inputs or truncated inputs.

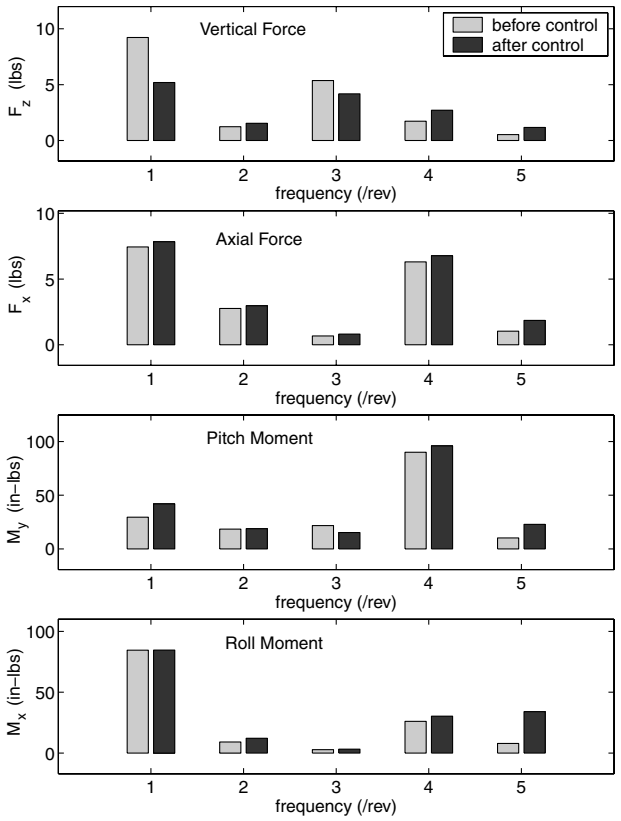

Fig. 8 Target reduction of 1/rev hub vertical force F_z: effect on hub loads.

F is a vector representing the fixed system hub loads harmonics. F_0 represents the uncontrolled fixed system hub forces and moments; γ is a vector containing the N_b individual flap inputs, and T is a $(12N_h) \times (2N_bN_h)$ transfer matrix to control N_h harmonics. Note that this model assumes that the fixed system hub loads are periodic. In a previous study [20], F and γ were expressed as time samples instead of harmonics, and the controller was tested analytically using a comprehensive helicopter simulation code. In the present study, the controller is tested in real time, and harmonics are used instead of time samples to reduce the size of the matrices in the identification problem.

Using this global model, the identification problem involves determination of the transfer matrix, given the control inputs and measured vibration outputs. The transfer matrix varies with helicopter operating conditions (e.g., thrust, airspeed). Therefore, the identification method should be made on-line to track the transfer matrix in real time. In the present study, the Kalman filter method is used. It is a computationally efficient algorithm designed to update parameter estimates recursively on the basis of a single measurement. Although the uncontrolled vibration vector F_0 can be obtained from measurements with no flap control inputs, it should be estimated along with the transfer matrix T because it will vary with flight conditions and helicopter characteristics. Equation (1) can then be rewritten as

$$F = [TF_0]\begin{Bmatrix}\gamma\\1\end{Bmatrix} \tag{2}$$

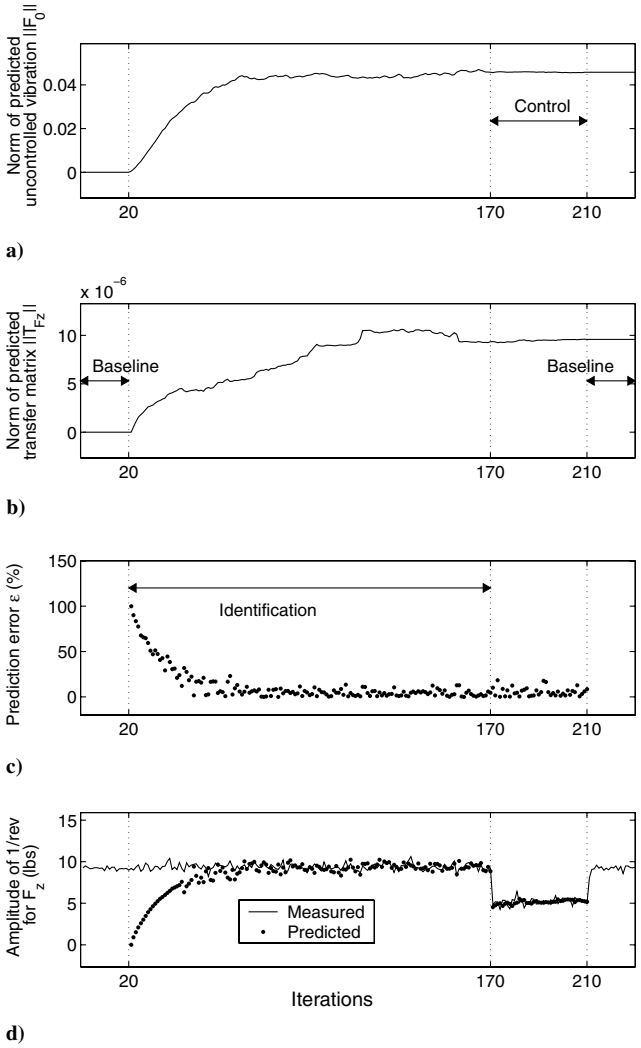

Fig. 9 Target reduction of 1/rev hub vertical force F_z: time history of various parameters.

At any iteration n, the typical form for the jth measurement is (measurement model)

$$(F_j)_n = [\gamma_n 1]\begin{Bmatrix} (T_j)_n^T \\ (F_{0j})_n \end{Bmatrix} \tag{3}$$

The above equation is of the form:

$$z_n = H_n x_n + v_n \tag{4}$$

where (T_j) is the jth row of T. Following the notations used in [22], z_n is the measurement vector, x_n is the state vector to be estimated, and H_n represents the measurement matrix. The measurement noise v_n is also included in the measurement model and is assumed to be a zero mean, white sequence of constant covariance r. For simplicity, the subscript j is omitted in these notations. Because the loads are periodic, the state vector dynamics (system model) is assumed quasi static and is written as

$$x_n = x_{n-1} + w_{n-1} \tag{5}$$

where w_{n-1} is the process noise, assumed to be a zero-mean, white sequence of constant covariance Q. Based on the measurement and system models, the Kalman filter discrete equations for updating state estimates are written as

Kalman gain matrix:

$$K_n = P_{n-1}H_n^T\left[H_n P_{n-1} H_n^T + r\right]^{-1} \tag{6}$$

Error covariance update:

$$P_n = [I - K_n H_n][P_{n-1} + Q] \tag{7}$$

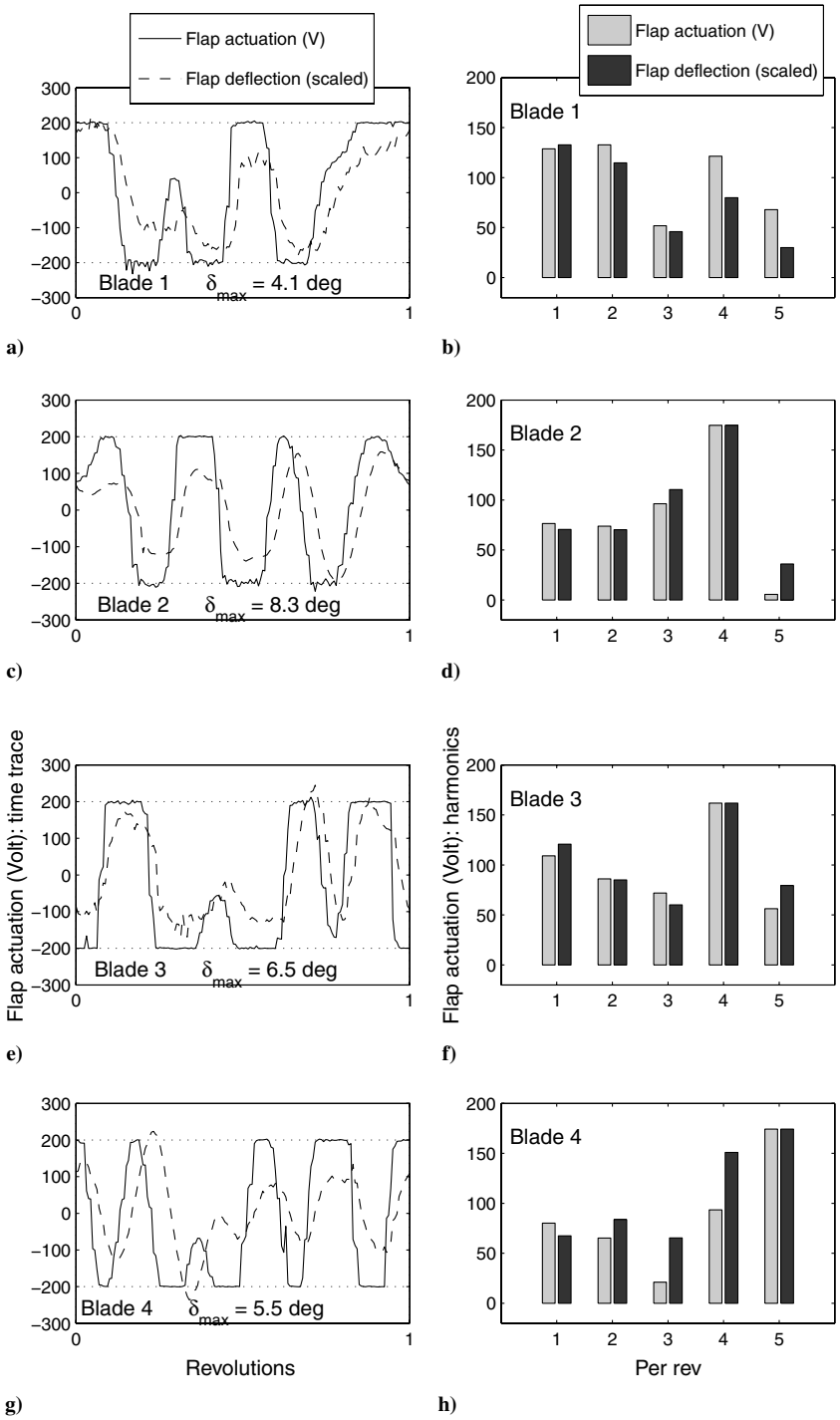

Fig. 10 Target reduction of 1/rev hub vertical force F_z: optimal flap inputs.

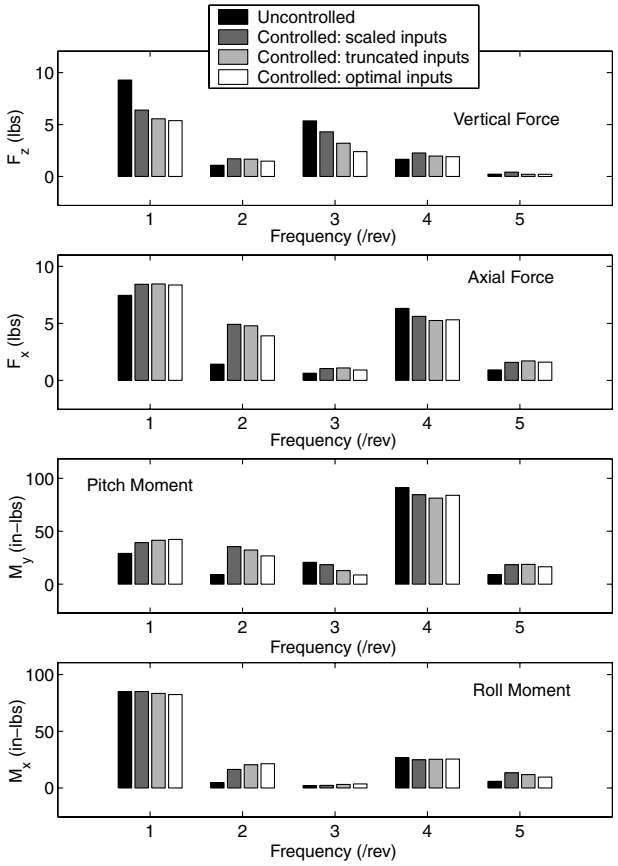

Fig. 11 Predicted reduction of 1/rev hub vertical force F_z using different limiting methods.

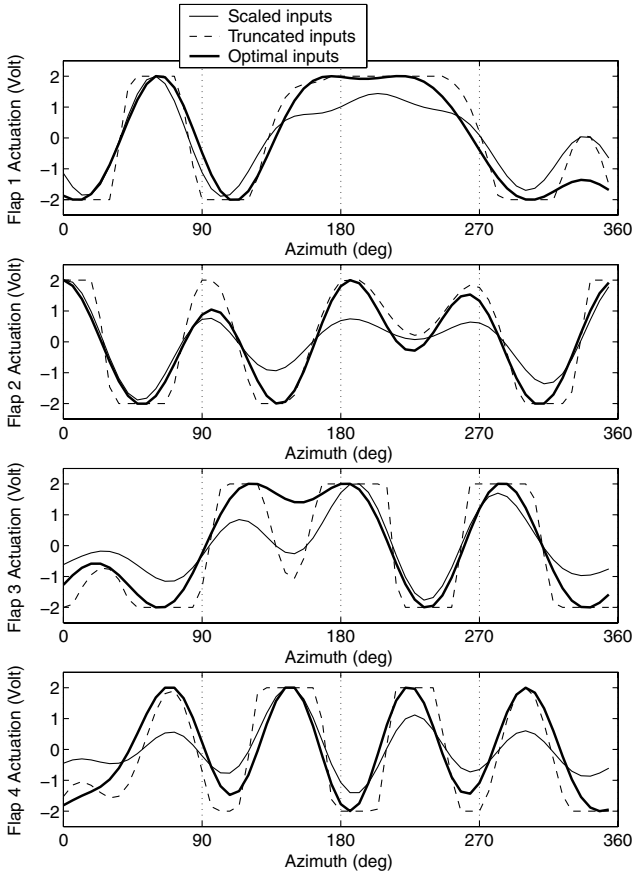

Fig. 12 Predicted reduction of 1/rev hub vertical force F_z using different limiting methods: optimal flap inputs.

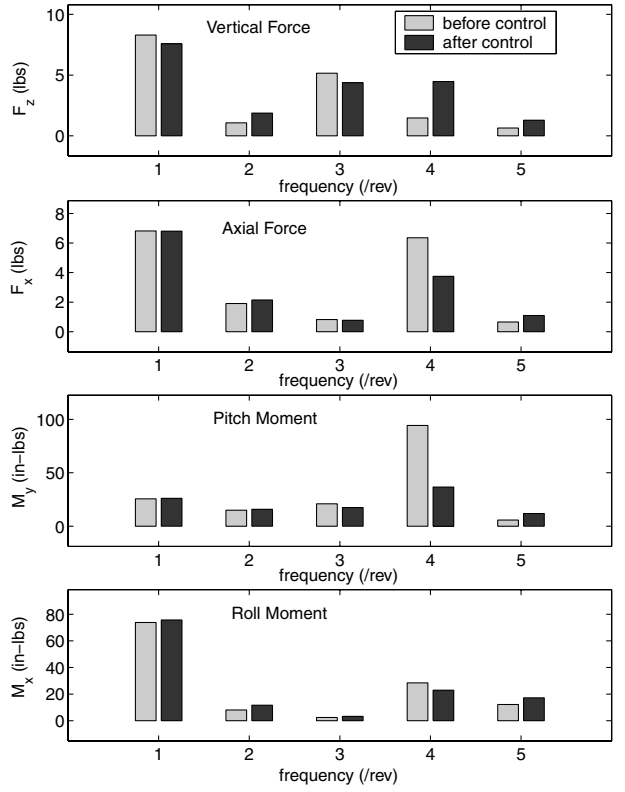

Fig. 13 Target reduction of 4/rev hub pitching moment M_y: effect on hub loads.

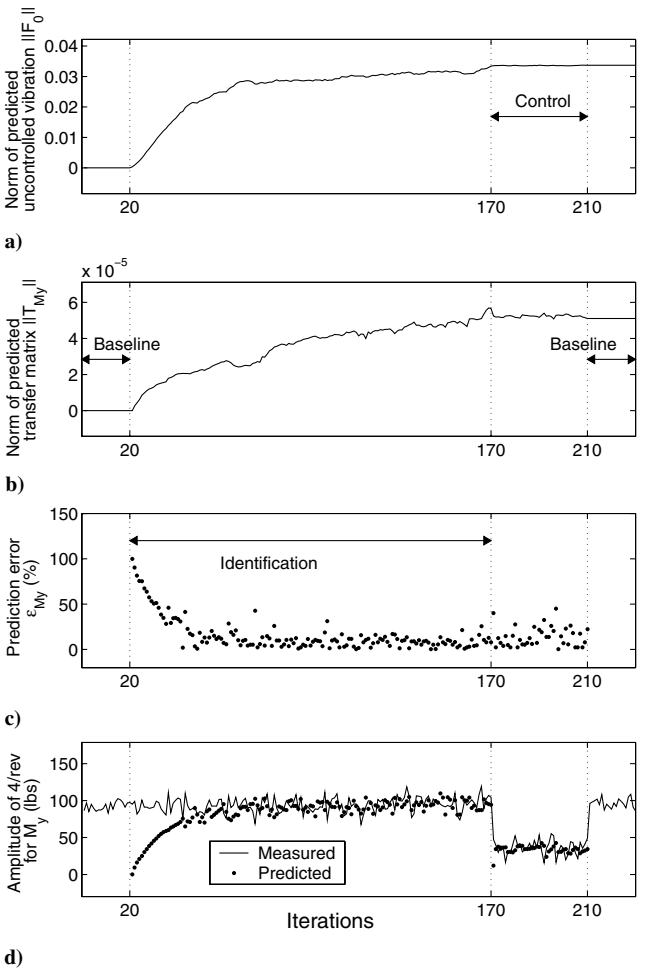

Fig. 14 Target reduction of 4/rev hub pitching moment M_y: time history of various parameters.

State estimate update:

$$x_n = x_{n-1} + K_n(z_n - H_n x_{n-1}) \tag{8}$$

Note that the Kalman gain vector K_n is the same for all j measurements, so that the unknown parameters $[TF_0]$ can be identified in a single step:

$$[TF_0]_n = [TF_0]_{n-1} + \left(F_n - [TF_0]_{n-1}\begin{Bmatrix}\gamma_n \\ 1\end{Bmatrix}\right)K_n^T \tag{9}$$

This represents an important reduction in computation time because P_n and K_n are calculated only once for each time cycle, and the computation of K_n only requires inversion of a scalar. Once the state estimates are obtained, the optimal control inputs can be determined. In the present investigation, a deterministic controller is used. For this controller, all the model properties are known from the identification algorithm. The individual multicyclic controls are based on the minimization of the performance function J, expressed as

$$J = Y^T W_F Y + \gamma^T W_\gamma \gamma + \Delta\gamma^T W_{\Delta\gamma}\Delta\gamma \tag{10}$$

where $Y = F - F_{\text{obj}}$. For simplicity, the subscript n indicating the iteration number is omitted. The weighting matrices W_F, W_γ, and $W_{\Delta\gamma}$ are applied to the output response, the individual flap input controls, and the individual flap control rates, respectively. Typically, these are diagonal matrices. Some diagonal elements of W_F can be set to zero to keep the corresponding vibration component uncontrolled. W_γ limits the flap control amplitude, and $W_{\Delta\gamma}$ limits the control rate. In the present study, $W_{\Delta\gamma} = 0$ is used. The optimal control input for each blade is obtained from the minimization of the

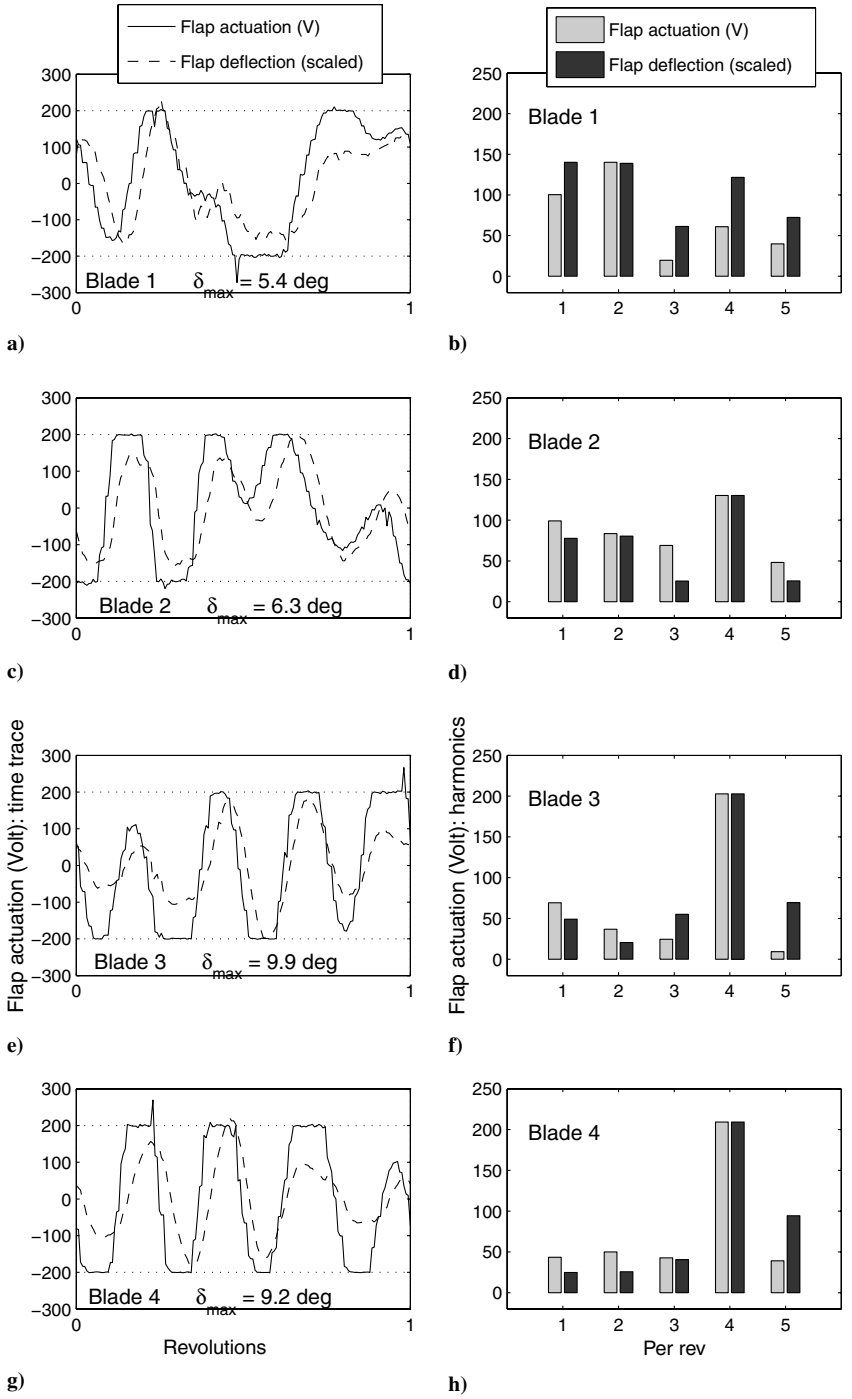

Fig. 15 Target reduction of 4/rev hub pitching moment M_y: optimal flap inputs.

performance function J, which means $\partial J/\partial \gamma = 0$. This results in the optimal control solution in the form (for $W_{\Delta\gamma} = 0$):

$$(\gamma^{\text{opt}})_n = -DT^T W_F Y_n \tag{11}$$

where $D = [T^T W_F T + W_\gamma]^{-1}$.

Because the matrix D is symmetric positive definite, the conjugate gradient method can be used to efficiently compute optimal weights, in order to decrease computation time.

The weight matrix associated with the flap actuation, W_γ, is a diagonal matrix. The choice of W_γ is important because it determines the amplitude of the control command. It is desired that the control commands remain below the maximum allowed value, $\gamma_{\max}$.

There are several ways to impose this constraint on the flap actuation:

1) Adjust (increase) the weights associated with the control inputs until their amplitude becomes lower than the maximum bound.

2) Apply a scaling factor to the command inputs which exceed $\gamma_{\max}$.

3) Truncate the command input whenever it exceeds the maximum.

However, none of these approaches solve the real problem, which can be formulated as

$$\gamma_{\text{optimal}} = \min \ \{\|F_0 + T \times \{\gamma_1\gamma_2\gamma_3\gamma_4\}^T - F_{\text{obj}}\|\}$$
$$\max_t(\gamma_k) < \gamma_{\max}, \qquad k = 1\text{–}4$$

where $\max_t(\gamma_k)$ signifies the maximum value of the control input for flap k expressed in the time domain over one revolution. This constrained minimization problem can be solved using Matlab function FMINCON, which uses a sequential quadratic programming (SQP) method. In this method, the function solves a QP subproblem at each iteration. An estimate of the Hessian of the Lagrangian is updated at each iteration using the Broyden–Fletcher–Goldfarb–Shanno (BFGS) formula [23,24]. This method yields the best results (minimum objective function), however, it may be too costly in computer time to use in a real-time application.

III. Experiment Setup

A. Active Rotor Model

To validate experimentally the proposed controller, a model rotor is fabricated. The rotor characteristics are summarized in Table 1. It is a four-bladed, Mach-scale rotor with one active trailing-edge flap on each blade.

The trailing-edge flaps are actuated using piezoelectric benders. Four actuators are manufactured using commercially available piezoelectric sheets of dimension 2 in × 1 in × 10 mils (PZT-5H). Actuators are fabricated following the design described in [25] by bonding together eight piezoceramic sheets on to a middle brass shim using a high performance adhesive. The piezoelectric sheets are of different lengths, resulting in a tapered actuator. The actuator is shown in Fig. 1. Electrical connections to the actuator layers are such that when the top ceramic sheets expand, the bottom ceramic sheets contract [in the plane of the lead zirconate titanate (PZT) sheets], resulting in a net bending of the actuator.

The motion of the actuator is magnified and transmitted to the flaps using a flexure-based leverage mechanism, as shown in Fig. 2. The flap articulation is realized by two tempered stainless steel shims, clamped on one side to the flap, and on the other side to the blade. The actuator motion is transmitted to the flap by means of a rod attached at the actuator tip which can glide inside a cusp attached to the flap. Details of the flexure hinge design can be found in [26].

The blades are untwisted and with a rectangular planform. They consist of a high-density foam core covered in a fiberglass skin. The anchor plate supporting the actuator and flap mechanism is glued to a graphite-epoxy composite spar, and leading edge weights are used to ensure that each blade section center of gravity is at the quarter-chord. A blade with a flexure-articulated flap is shown in Fig. 3.

B. Wind Tunnel

Testing was performed in the Glenn L. Martin wind tunnel at the University of Maryland. The blades are fitted to a one-seventh scale Bell-412 M-scaled rotor hub (shown in Fig. 4).

This hub consists of two composite yokes that are stacked perpendicular to each other. Each yoke can accommodate two blades. The yokes are designed to act as virtual hinges for flap and lead–lag motion. Blade feathering is achieved via an elastomeric pitch bearing. Two sets of elastomeric lag dampers are installed on each yoke to ensure aeroelastic stability. In addition to the yoke gages, the rotor rig is equipped with a six-component fixed frame balance. Data are transferred between the rotating and fixed frames though two slip rings, one for actuation and the other for sensing purposes. The rotor rpm is controlled by a variable speed, water-cooled, hydraulic motor and pump rated for 55 hp (maximum speed 6000 rpm). A belt and pulley arrangement connects the motor to the rotor shaft. The Mach-scaled operating speed for the Bell-412 rotor is 2000 rpm, however, for the present testing the operating speed was limited to 1500 rpm, in order to avoid damages to the flap flexures. The rotor installed in the wind-tunnel test section is shown in Fig. 5.

C. Controller Implementation

To implement the control algorithm, a dedicated computer (Pentium III, 550 MHz PC) is set up with a data acquisition board (National Instruments PCI-MIO-16E-1, 12-bit DAQ board) to host the controller and perform data acquisition and waveform generation. This provides an efficient system to implement the control algorithm in real time directly in Visual C++. Double buffering is used on the data acquisition board for simultaneously downloading the measurements from the previous iteration and uploading the command waveform for the next iteration to the data acquisition board. Data sampling and command uploading are synchronized to the rotor speed via a 60/rev tachometer (data are acquired and waveform is output at a rate of 60 data points per rotor

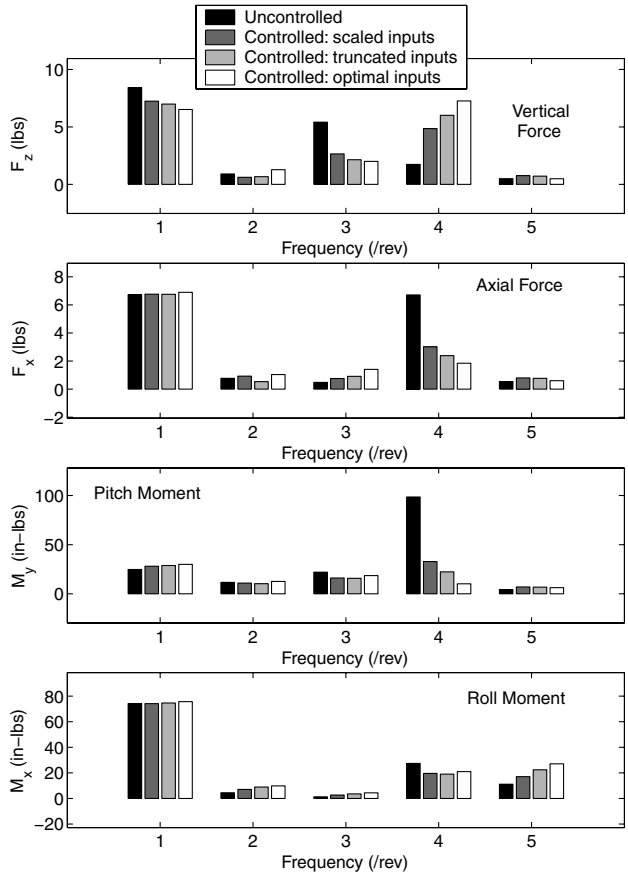

Fig. 16 Predicted reduction of 4/rev hub pitching moment M_y using different limiting methods.

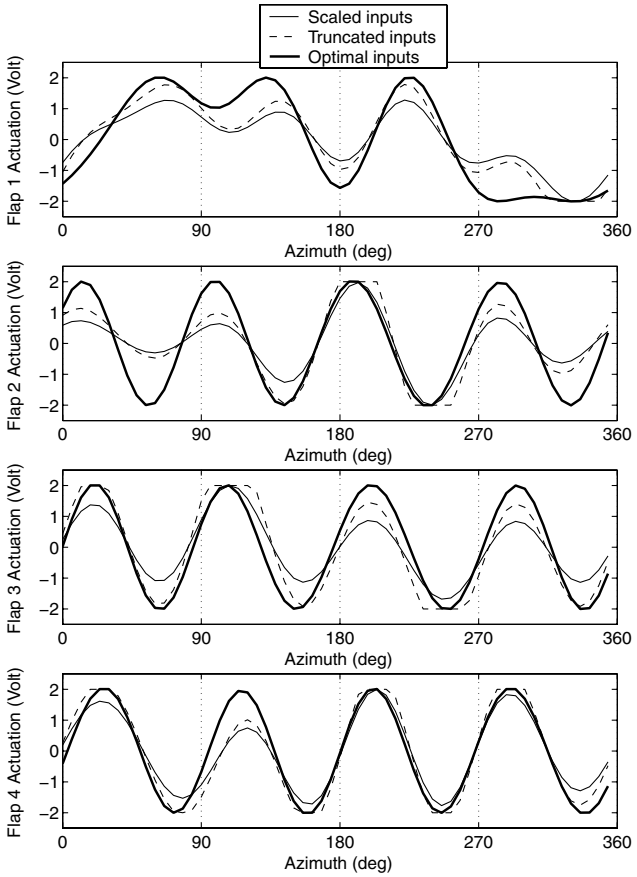

Fig. 17 Predicted reduction of 4/rev hub pitching moment M_y using different limiting methods: optimal flap inputs.

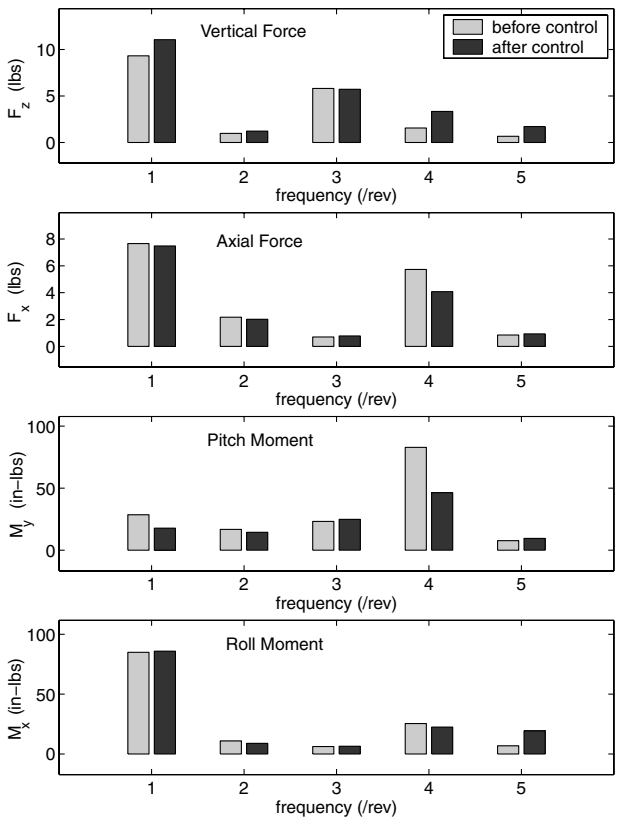

Fig. 18 Target reduction of 1 and 4/rev hub pitching moments M_y: effect on hub loads.

revolution). Starting of continuous data acquisition is triggered by the 1/rev signal from the rotor hub, which occurs when blade 1 is at the rotor azimuth 0 deg. A diagram of the controller is shown in Fig. 6.

IV. Test Results

This section describes closed-loop tests performed in the Glenn L. Martin wind tunnel, when the control objective is the

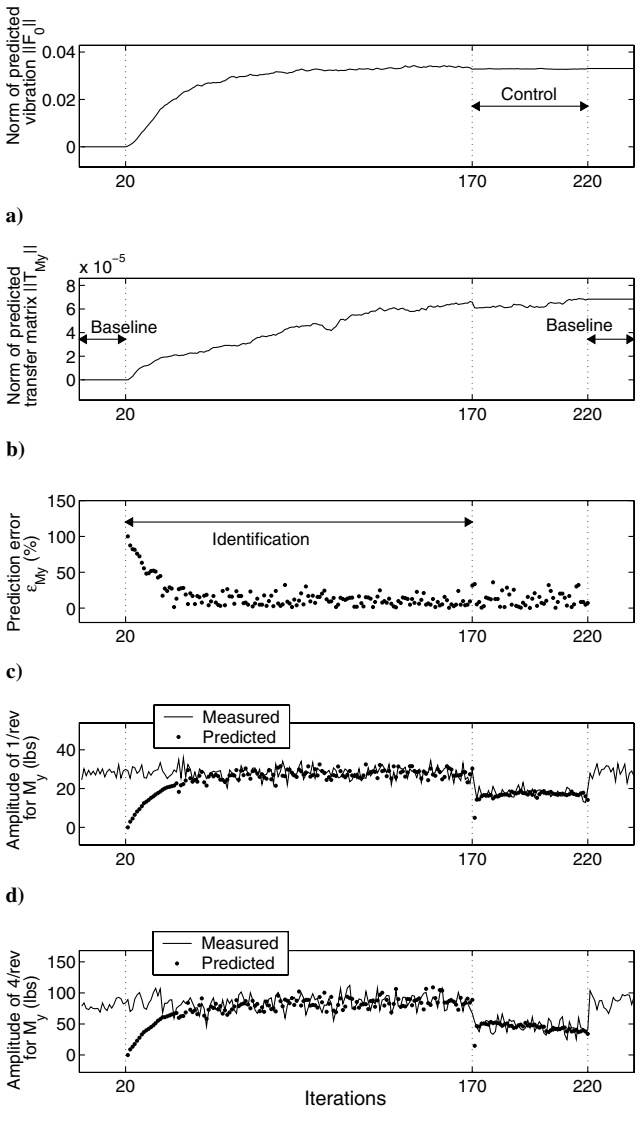

Fig. 19 Target reduction of 1 and 4/rev hub pitching moments M_y: time history of various parameters.

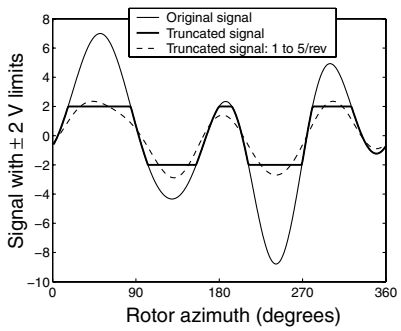

Fig. 20 Problem with filtering a truncated signal.

reduction of vibratory components of single or several fixed frame loads.

Tests are performed at the following flight condition:

1) rotor speed: 1500 rpm,

2) wind speed: 67 mph (advance ratio $\mu = 0.25$),

3) collective angle: 2 deg,

4) shaft tilt angle: 2 deg.

The rotor thrust under these conditions is equal to about 12 lb. Rotor mass imbalance is minimized by adding corrective weights at the root of the blades. However, it is difficult to correct aerodynamic differences between the blades. Therefore, the fixed frame loads contain components at frequencies other then $4/\text{rev}$, which can be included in the controller objective function.

Cyclic angles are adjusted before each closed-loop test to minimize the $1/\text{rev}$ blade root bending moments in the rotating frame and subsequently left unchanged during the test. For all tests in this section, the flap actuation is maintained within the ± 200-V limits by using truncated inputs, as illustrated in Fig. 7.

Each test consists of four phases, defined as follows and carried out in sequence:

1) baseline: no command inputs to the flaps,

2) identification: inputs of varying amplitude, frequency, and phase are used to identify the transfer matrices,

3) control: optimal inputs are generated, closed-loop control and system identification are performed simultaneously,

4) back to baseline: no command inputs to the flaps.

The maximum achievable actuator deflection was not large enough to achieve simultaneous reduction of all harmonics for all the loads. The objective function was therefore limited to target only a few selected harmonics. The following sections

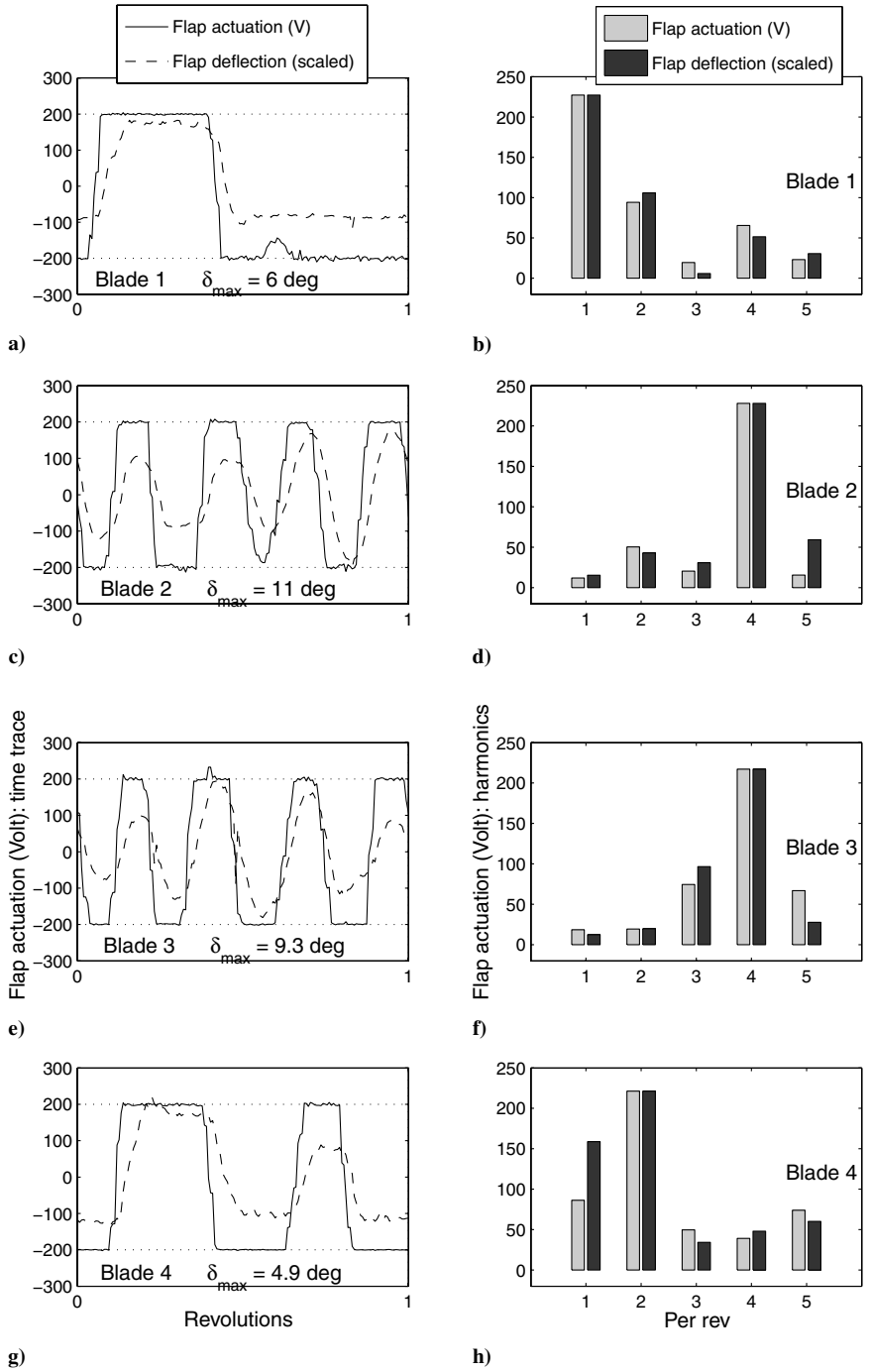

Fig. 21 Target reduction of 1 and $4/\text{rev}$ hub pitching moments M_y: optimal flap inputs.

describe three tests for which significant vibration reduction was achieved.

A. Test 1: Reduction of Normal Force Vibration at 1/rev

Figures 8–10 describe a closed-loop test when the control objective is the reduction of the 1/rev component of the vertical hub load. Figure 8 shows the magnitude of vibratory hub loads before and after control. At this flight condition, the vertical hub load before control consists of a dominant 1/rev harmonic component (about 10 lb), and smaller 3/rev (about 5 lb) and 4/rev (about 1.5 lb) components. After control, the 1/rev component is reduced by about 50%. However, this reduction in vertical vibration is accompanied by an increase in 1/rev vibration for the pitching moment (by about 40%). Although not included in the cost function, the 3/rev component of the normal force is also reduced by 25%. Other harmonics of the vertical hub force have increased.

Figures 9a–9c show the time history of identified parameters, and Fig. 9d shows the time history of the objective function during the test. Control inputs after convergence are shown in Fig. 10. Flap actuation signals are truncated for all blades. All harmonics (from 1to 5/rev) appear to be important, with a dominant 4/rev component for blades 2 and 3. The controller attempts to generate a 1/rev component in the fixed frame to counteract the existing vibration. There are several ways to generate this 1/rev component, not only using low frequency flap inputs, but also using dissimilar blade actuations (at any frequency). The controller computes the solution which also minimizes the flap actuation amplitude.

For this test, the actuation signal is truncated whenever the controller generates a signal exceeding the maximum allowable value (± 200 V). Figures 11 and 12 compare the predicted controller performance using different methods to apply limits: using scaled inputs, using truncated inputs, and solving the constrained minimization problem using the Matlab function FMINCON, based on the SQP method. Figure 11 shows the vibration levels before control and predicted vibration levels after control. Predictions are obtained using the linear model identified during the test. Using this model, vibration reduction improves when using truncated inputs compared to using scaled inputs and further improves when solving the problem using the SQP method. Note that predicted vibration using truncated inputs is very close to measured values, but does not match exactly with test data. This is because the actual flap actuation is truncated and therefore contains harmonics higher than 5/rev, while the model used for prediction assumes this input consists of harmonics from 1 to 5/rev. Figure 12 compares flap actuation signals obtained with the three methods. The actuation command is plotted before amplification (by a factor of 100). The signals are very similar in phase, but significant differences in amplitude are apparent. Note that the optimal inputs generated using the SQP method appear close to a truncated signal (signal becomes flat near ± 2-V limits).

B. Test 2: Reduction of Pitching Moment Vibration at 4/rev

Figures 13–15 describe a closed-loop test when the control objective is the reduction of the 4/rev component of the fixed frame pitching moment. The pitching moment vibration at the rotor hub can be a large contributor to vibration at the pilot seat station in the fuselage [27].

Figure 13 shows the harmonics of hub loads before and after control. After control, the 4/rev component of the hub pitching moment is reduced by 62%. Other harmonics of M_y as well as other hub loads are also affected by the control inputs. The 4/rev component of the axial vibration is reduced (by about 40%); however, the 4/rev component of the vertical force is increased by a factor of 3, from 1.5 to 4.5 lb. Figure 14 shows the evolution of some identification parameters during the test as well as the time history of the pitching moment 4/rev component. Optimal control inputs generated are shown in Fig. 15. Actuation for flaps 2, 3, and 4 have a dominant 4/rev component, with similar phase. The relatively large 1 and 2/rev actuation components for blades 1 and 2 are unexpected, since harmonics below 3/rev would not produce any 4/rev vibration in the fixed frame. One explanation lies in the way saturation limits are imposed, in this case by truncating the actuation command when it exceeds the maximum allowable voltage. When saturation limits are imposed by solving the constrained optimization problem, the optimal inputs contain much smaller 1 and 2/rev components, particularly for blade 2 (Fig. 15).

Figures 16 and 17 compare the predicted controller performance using different methods to apply limits. Figure 16 shows the vibration levels before control and predicted vibration levels after control. Similar to the previous study for vertical vibration, improvements in 4/rev hub pitching moment vibration reduction are predicted using the SQP method. The 4/rev component is reduced by 90% compared to the measured 62%. However, a large increase in the 4/rev normal force is also predicted. Figure 17 compares flap actuation signals (before amplification) obtained with the three methods. It is interesting to observe that the optimal inputs generated by the SQP method, which yields the best results, are very close to phase-shifted 4/rev signals, except for blade 1.

C. Test 3: Reduction of Pitching Moment Vibration at 1 and 4/rev

Figures 18–21 describe a closed-loop test when the control objective is the simultaneous reduction of the 4 and 1/rev components of the fixed frame pitching moment. Figure 18 shows vibration harmonics before and after control for several hub loads. The 1/rev component is reduced by 38% and the 4/rev component by 44%. Some reduction is also observed in the 4/rev component of the axial hub load (29%). However, this is accompanied by an increase in vibratory components of the vertical hub load: the 1/rev increases by 18% and the 4/rev is more than doubled. Figure 19 shows the time history of several identified parameters, prediction error, as well as the time history of the 1 and 4/rev components for the target hub load. Note that just at the beginning of the control phase, predicted vibration reduction is very good: over 80% for both 1 and 4/rev components. However, actual vibration reduction is only about 20 and 40%, respectively. This is because prediction is based

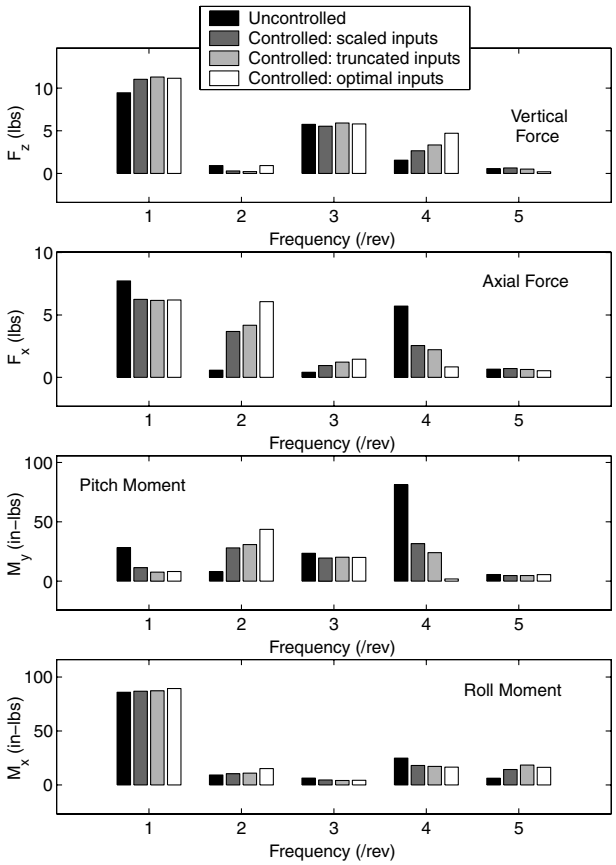

Fig. 22 Predicted reduction of 1 and 4/rev hub pitching moments M_y using different limiting methods.

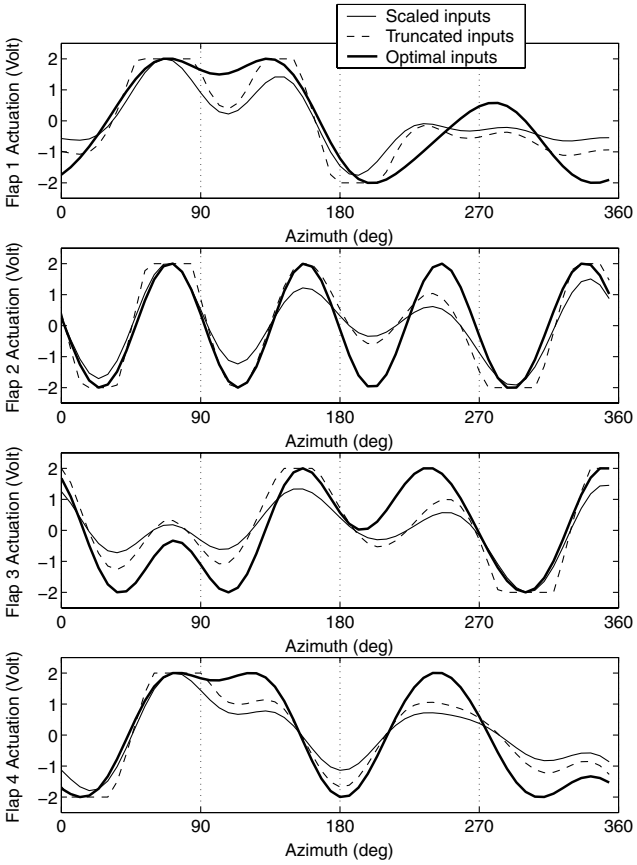

Fig. 23 Predicted reduction of 1 and 4/rev hub pitching moments M_y using different limiting methods: optimal flap inputs.

on filtered harmonic components (1 to 5/rev) of the truncated signal, and not the truncated signal itself. As illustrated in Fig. 20, the peak-to-peak amplitude of the filtered signal can be much larger than that of the truncated signal, hence the overprediction of vibration reduction. The resulting decrease in the transfer matrix norm can be observed in Fig. 19b at iteration 170. The norm of identified T_{PIT} increases during control and correspondingly the 4/rev reduction improves: at the end of the control phase (after 50 iterations), the 4/rev is reduced by 55%. The optimal flap inputs generated by the controller are shown in Fig. 21. Deflections for flaps 2 and 3 are dominated by a large 4/rev component at the same phase. Deflections for flap 1 are largely at the 1/rev frequency, and for flap 4 at the 2/rev frequency.

Figures 22 and 23 compare the predicted controller performance using different methods to apply limits. Figure 22 shows the vibration levels before control and predicted vibration levels after control. Similar to the previous two tests, using the SQP method results in improved vibration reduction: the 4/rev component is reduced by 97% compared to the measured 44%, and the 1/rev component is reduced by 71% compared to the measured 38%. Figure 23 compares the flap actuation signals computed with the three methods (before amplification).

Table 2 summarizes the results from the previous three tests.

V. Summary and Conclusions

This paper describes wind-tunnel testing of a new controller to reduce helicopter vibrations using trailing-edge flaps. This new controller takes into account rotor dissimilarities and allows different control inputs to be applied to each trailing-edge flap.

The controller's ability to minimize fixed frame vibratory loads at both 4 and 1/rev frequencies is investigated in forward flight. A four-bladed Mach-scaled rotor with piezobender trailing-edge flaps is used for this investigation, with all four flaps active simultaneously. Closed-loop tests are conducted in the Glenn L. Martin wind tunnel, at a rotor speed of 1500 rpm, and advance ratio 0.25. The key conclusions are as follows:

1) With collective blade angle of 2 deg, the hub normal force consists of large 1 and 3/rev components and a smaller 4/rev component. The 1/rev component is reduced by about 50%. However, this is accompanied by an increase in the 1/rev component of other loads.

2) The hub pitching moment vibration consists mainly of a large 4/rev component and a small 1/rev component. The 4/rev component can be reduced by over 60%. This is accompanied by a reduction in the 4/rev hub rolling moment and axial force; however, the 4/rev normal force is increased.

3) Solving the minimization problem with nonlinear constraints yields much improved results. However, this procedure is very time consuming and cannot be implemented in real time during the wind-tunnel testing with the computer available.

Acknowledgments

The authors gratefully acknowledge the support for this research work provided by the NASA Ames Research Center with Technical Monitor, William Warmbrodt. The authors would also like to thank all the students and researchers of the Alfred Gessow Rotorcraft Center for their help during testing.

References

[1] Friedmann, P. P., and Millott, T. A., "Vibration Reduction in Rotorcraft Using Active Control: A Comparison of Various Approaches," *Journal of Guidance, Control, and Dynamics*, Vol. 18, No. 4, July–Aug. 1995, pp. 664–673.

[2] Nguyen, K., and Chopra, I., "Application of Higher Harmonic Control to Rotors Operating at High Speed and Thrust," *Journal of the American Helicopter Society*, Vol. 35, No. 3, 1990, pp. 78–89.

[3] Hammond, C. E., "Wind Tunnel Results Showing Rotor Vibratory Loads Reduction Using Higher Harmonic Blade Pitch," *Journal of the American Helicopter Society*, Vol. 28, No. 1, Jan. 1983, pp. 10–15.

[4] Shaw, J., Albion, N., Hanker, E. J., and Teal, R. S., "Higher Harmonic Control: Wind Tunnel Demonstration of Fully Effective Vibratory Hub Forces Suppression," *Journal of the American Helicopter Society*, Vol. 34, No. 1, Jan. 1989, pp. 14–25.

[5] Nguyen, K., Betzina, M., and Kitaplioglu, C., "Full-Scale Demonstration of Higher Harmonic Control for Noise and Vibration Reduction on the XV-15 Rotor," *Journal of the American Helicopter Society*, Vol. 46, No. 3, July 2001, pp. 182–191.

[6] Wood, E. R., Powers, R. W., Cline, C. H., and Hammond, C. E., "On Developing and Flight Testing a Higher Harmonic Control System," *Journal of the American Helicopter Society*, Vol. 30, No. 1, Jan. 1985, pp. 3–20.

[7] Ham, N. D., "Helicopter Individual Blade Control and its Applications," *American Helicopter Society 39th Annual Forum*, American Helicopter Society International, Alexandria, VA, May 1983, pp. 613–623.

Table 2 Test results summary

Control objective	θ_0	Measured vibration reduction	Predicted vibration reduction		
			Scaled inputs	*Truncated inputs*	*Optimized inputs*
F_z, 1/rev	2 deg	50%	31%	40%	42%
M_y, 4/rev	2 deg	62%	67%	77%	90%
M_y, 1 and 4/rev	2 deg	43%	61%	71%	90%

[8] Guinn, K. F., "Individual Blade Control Independent of a Swashplate," *Journal of the American Helicopter Society*, Vol. 27, No. 3, July 1982, pp. 25–31.

[9] Richter, P., and Blaas, A., "Full Scale Wind Tunnel Investigation of an Individual Blade Control System for the BO-105 Hingeless Rotor," *19th European Rotorcraft Forum*, American Helicopter Society International, Alexandria, VA, Sept. 1993, pp. G5.1–G5.12.

[10] Jacklin, S. A., Nguyen, K., Blaas, A., and Richter, P., "Full-Scale Wind Tunnel Test of a Helicopter Individual Blade Control System," *American Helicopter Society 50th Annual Forum*, American Helicopter Society International, Alexandria, VA, May 1994, pp. 579–596.

[11] Chopra, I., "Status of Application of Smart Structures Technology to Rotorcraft Systems," *Journal of the American Helicopter Society*, Vol. 45, No. 4, Oct. 2000, pp. 228–252.

[12] Straub, F. K., "A Feasibility Study of Using Smart Materials for Rotor Control," *Smart Materials and Structures*, Vol. 5, No. 1, Feb. 1996, pp. 1–10.

[13] Prechtl, E. F., and Hall, R. S., "Design of a High Efficiency, Large Stroke, Electromechanical Actuator," *Smart Materials and Structures*, Vol. 8, No. 1, Feb. 1999, pp. 13–30. doi:10.1088/0964-1726/8/1/002

[14] Millott, T. A., and Friedmann, P. P., "Vibration Reduction in Helicopter Rotors Using an Active Control Surface Located on the Blade," *33rd AIAA/ASME/ASCE/AHS/ASC Structures, Structural Dynamics and Materials Conference*, AIAA, New York, 13–15 April 1992, p. 1975.

[15] Milgram, J., and Chopra, I., "Parametric Design Study for Actively Controlled Trailing Edge Flaps," *Journal of the American Helicopter Society*, Vol. 43, No. 2, 1998, pp. 110–115.

[16] Koratkar, N. A., and Chopra, I., "Wind Tunnel Testing of a Smart Rotor Model with Trailing-Edge Flaps," *Journal of the American Helicopter Society*, Vol. 47, No. 4, 2002, pp. 263–272.

[17] Spencer, M. G., Sanner, R. M., and Chopra, I., "Adaptive Neurocontrol of Simulated Rotor Vibrations Using Trailing Edge Flaps," *Journal of Intelligent Material Systems and Structures*, Vol. 10, No. 11, 1999, pp. 855–871. doi:10.1106/RX0W-UJ7M-QEL9-E58P

[18] Spencer, M. G., Sanner, R. M., and Chopra, I., "Closed-Loop Neurocontroller Tests on Piezoactuated Smart Rotor Blades in Hover," *AIAA Journal*, Vol. 40, No. 8, 2002, pp. 1596–1602.

[19] Spencer, M. G., Sanner, R. M., and Chopra, I., "Adaptive Neurocontroller for Vibration Suppression and Shape Control of a Flexible Beam," *Journal of Intelligent Material Systems and Structures*, Vol. 9, No. 3, 1998, pp. 160–170.

[20] Roget, B., and Chopra, I., "Individual Blade Control Methodology for a Rotor with Dissimilar Blades," *Journal of the American Helicopter Society*, Vol. 48, No. 3, July 2003, pp. 176–185.

[21] Roget, B., and Chopra, I., "Closed Loop Testing of a Rotor with Individually Controlled Trailing-Edge Flaps for Vibration Reduction," *American Helicopter Society 61st Annual Forum*, American Helicopter Society International, Alexandria, VA, June 2005.

[22] Gelb, A., Kasper, J. F., Nash, R. A., Price, C. F., and Sutherland, A. A., *Applied Optimal Estimation*, MIT Press, Cambridge, MA, 1974, p. 110.

[23] Fletcher, R., and Powell, M. J. D.,"A Rapidly Convergent Descent Method for Minimization," *Computer Journal*, Vol. 6, No. 2, July 1963, pp. 163–168.

[24] Goldfarb, D., "A Family of Variable Metric Updates Derived by Variational Means," *Mathematics of Computing*, Vol. 24, No. 109, Jan. 1970, pp. 23–26.

[25] Koratkar, N., "Smart Helicopter Rotor with Piezoelectric Bender Actuated Trailing-Edge Flaps," Ph.D. Thesis, Aerospace Department, University of Maryland, College Park, MD, 2000.

[26] Roget, B., and Chopra, I., "Wind Tunnel Testing of an Individual Blade Controller for a Dissimilar Rotor," *American Helicopter Society 60th Annual Forum*, American Helicopter Society International, Alexandria, VA, June 2004.

[27] Yeo, H., and Chopra, I.,"Coupled Rotor/Fuselage Vibration Analysis Using Detailed 3-D Airframe Models," *Mathematical and Computer Modelling*, Vol. 33, Nos. 10–11, 2001, pp. 1035–1054. doi:10.1016/S0895-7177(00)00299-5